ELSEVIER

Coordination Chemistry Reviews 233–234 (2002) 273–287

COORDINATION CHEMISTRY REVIEWS

www.elsevier.com/locate/ccr

Iron complexes of borylated vicinal dioxime macrocycles

Dennis V. Stynes *, Isak Vernik, Fabio Zobi

Department of Chemistry, York University, Toronto, ON, Canada M3J 1P3

Received 5 October 2001; accepted 4 March 2002

Contents

Abstract

Metal complexes of the general form *trans*-FeN_4LL', where N_4 is a planar tetradentate macrocycle and L and L′ axial monodentate ligands form an important class of inorganic substances. This review summarizes the chemistry of low spin Fe(II) and μ-oxo Fe(III) complexes containing vicinal dioximate ligands with emphasis on the borylated forms; $Fe(DMGBF_2)_2$, $Fe(DMGBPh_2)_2$, $Fe(BQDBF_2)_2$, $Fe(NPQBF_2)_2$. An extensive range of binding affinities, ligand labilities, MLCT spectra, and redox potential may be achieved by variation in L, N_4, and BR_2 groups. Structural and ligand binding data for Fe(II) and μ-oxo Fe(III) complexes are discussed. The $Fe(DMGBR_2)_2$ complexes adopt either a C_{2v} or C_{2h} conformation depending upon the axial ligands present. Applications to the measurement, understanding, and use of nonbonded interactions are described.

Keywords: Iron dioxime; Oxo ligation; Kinetics; Nonbonded effects

* Corresponding author. Tel.: +1-416-736-2100; fax: +1-416-736-5936.
E-mail address: stynes@yorku.ca (D.V. Stynes).

0010-8545/02/$ - see front matter
PII: S0010-8545(02)00082-6

1. Abbreviations

FeN_4	a planar bis(dioximato)iron(II) complex, $Fe(DMGBF_2)_2$ etc.
N_4	a dianionic planar tetradentate macrocyclic ligand, $(DMGBF_2)_2$ etc.
dioxH a vicinal dioximate ligand	dioxBR$_2$ a borylated vicinal dioximate ligand
DMGH dimethylglyoximate	$DMGBF_2$ (dimethylglyoximato)difluoroborate
	$DMGBPh_2$ (dimethlyglyoximato)diphenylborate
	$DMGBH_2$ (dimethylglyoximate)dihydridridoborate
	DMGBBN (dimethylglyoximato)bicyclononylborate
DPGH diphenylglyoximate	$DPGBF_2$ (diphenylglyoximato)difluoroborate
BQDH benzoquinone dioximate	$BQDBF_2$ (benzoquinonedioximato)difluoroborate
NPQH naphthoquinone dioximate	$NPQBF_2$ (naphthoquinonedioximato)difluoroborate

Axial ligands	
PY	pyridine
MeIm	1-methylimidazole
PIP	piperidine
PT	phthalonitrile
NPT	4-nitrophthalonitrile
DDQ	2,3-dichloro-5,6-dicyano-1,4-benzoquinone
TCNE	tetracyanoethylene
$MePz^+$	*N*-methylpyrazinium ion
2-$CNPYMe^+$	2-cyano-*N*-methylpyridinium ion
THF	tetrahydrofuran
DMSO	dimethylsulfoxide
DIB 1,4	diisocyanobenzene
TPP′	tetrakis(4-methoxyphenyl)porphyinate
Pc	phthalocyaninate
salen	bis(salicylaldehyde)ethylenediimine
Me_2BBZ	bis(dimethylbenzimidazole)

2. Introduction

Dimethylglyoxime [1] is a well known ligand commonly used in the analysis for nickel. The insoluble red $Ni(DMGH)_2$ complex was originally described by Tschugaev in 1905 [2]. While not a biochemical ligand as such, bis-glyoximes provide a planar tetracoordinate nitrogen environment analogous to that found in the corrin ring of vitamin B_{12} and the porphyrin ring of heme systems. Extensive studies of 'cobaloximes' beginning in the 1960s made use of $Co(DMGH)_2$ as a substitute for the naturally occurring cobalt corrin ring system [3,4].

Relatively few studies of $Fe(DMGH)_2$ complexes appeared during that time. Early studies of $Fe(dioxH)_2$ complexes included an erroneous report of reversible oxygen binding [5], a study of the reversible coordination of CO to diphenylglyoxime complexes [6], and the crystal structure of the $Fe(DMGH)_2(imidazole)_2$ complex [7]. The rich charge transfer [8,9] and Mossbauer spectra [10] of the iron derivatives also received attention.

The air sensitive $Fe^{II}(DMGH)_2(PY)_2$ complex forms when iron(II) salts are added to solutions containing dimethylglyoxime and pyridine under anaerobic conditions.

$$Fe^{2+} + 2DMGH_2 + 4PY \Rightarrow Fe(DMGH)_2(PY)_2 + 2PYH^+ \quad (1)$$

Pang [11] and Chen [12] described a variety of complexes

of the form $Fe(DMGH)_2LL'$ where L or L′ are ligands such as pyridine, methylimidazole, CO, phosphines, or isocyanides and reported extensive data on the kinetics of their ligand substitution reactions. Analogous chemistry is found for benzoquinone ($Fe(BQDH)_2$)and napthoquinone ($Fe(NPQH)_2$) dioxime systems [13,14]. Separation of sym- and asym-isomers of $Fe(NPQH)_2(DIB)(PY)$ and the binuclear $[Fe(NPQH)_2(PY)]_2(DIB)$ diisocyanobenzene bridged complex is reported by Lefko [15].

This review summarizes more recent advances in the chemistry of iron glyoximes complexes primarily from the author's lab. The extension of iron dioxime chemistry to weak ligand complexes, ferric derivatives, and oxo bridged species has been largely possible through the use of borylated dioximes.

3. Borylated dioximes

Schrauzer [16] first reported borylation of the bridging oximate protons in the reaction of $Ni(DMGH)_2$ with BF_3 to give $Ni(DMGBF_2)_2$. In the case of iron the reaction with BF_3 instead leads to a tris-clathrochelate complex (**1**).

$$Fe^{2+} + 3DMGH_2 + 2BF_3 \Rightarrow Fe(DMG)_3(BF)_2 + 4HF + 2H^+ \quad (2)$$

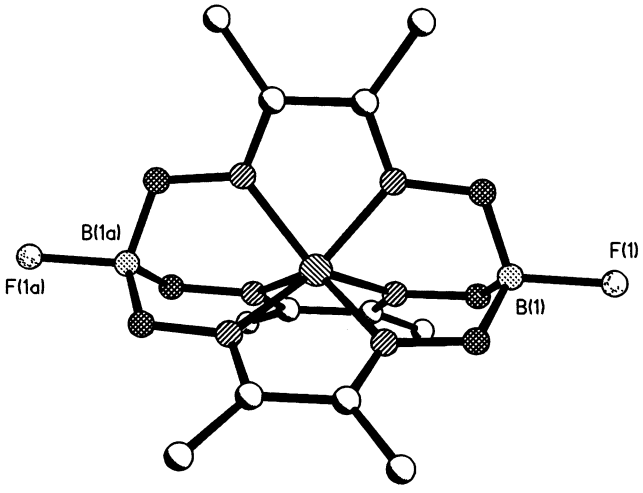

1

A variety of cobalt and iron [17,18] tris-clathrochelates have been studied. They are exceptionally stable, coordinatively saturated, and inert complexes which have had wide application as outer sphere electron transfer agents but they are not suitable for studies of ligand binding.

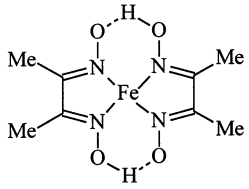

$Fe(dmgH)_2$

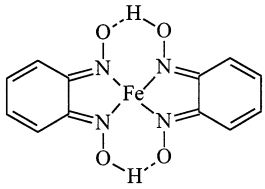

$Fe(bqdH)_2$

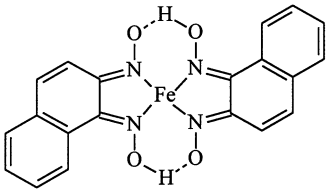

$Fe(npqH)_2$

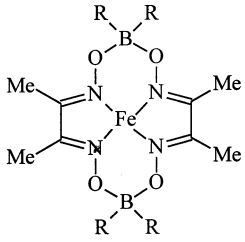

$Fe(dmgBR_2)_2$

Fig. 1. Bis-(dioximato)iron(II) complexes.

Thompson was the first to obtain bis-difluoroborylated iron dioxime complexes, [19] by reaction of the inert $Fe(dioxH)(PY)(CO)$ with BF_3, diox, DMG, BQD, or NPQ (Fig. 1).

$$Fe(dioxH)_2(PY)(CO) + 2BF_3 \Rightarrow Fe(dioxBF_2)_2(PY)(CO) + 2HF \quad (3)$$

Careful attention to the reaction work up is required if the more stable clathrochelate species is to be avoided in the dimethylglyoxime case. Diphenylborylated ($Fe(DMGBPh_2)_2$), hydroborated ($Fe(DMGBH_2)_2$), and borabicyclononane ($Fe(DMGBBN)_2$) analogues [19–23] are obtained using $[BPh_2]_2O$, BH_3–Et_2S, or borabicyclononane, respectively as the borylating agents in reaction (3) (see Fig. 2). The carbonyl ligand is replaced by heating or photolysis in the presence of excess pyridine. The very useful and labile acetonitrile complex, which is unknown for the parent $Fe(DMGH)_2$ system, is obtained by reaction with dilute aqueous acid in acetonitrile solution.

$$Fe(DMGBF_2)_2(PY)_2 + 2CH_3CN + 2H^+ \Rightarrow Fe(DMGBF_2)_2(CH_3CN)_2 + 2PYH^+ \quad (4)$$

A variety of ligated derivatives, $Fe(DMGBF_2)_2LL'$, where L and L′ may be virtually any monodentate ligand are then obtained by simple ligand substitution reactions.

Borylation significantly alters the character of the glyoxime ligand. The $Fe^{3+/2+}$ potential is raised by almost 700 mV depending upon the BR_2 group rendering the Fe(II) complexes generally air stable in solution. Trends in the $Fe^{3+/2+}$ potential versus BR_2 and axial ligands are as follows [21] ($E_{1/2}$ V vs. SCE):

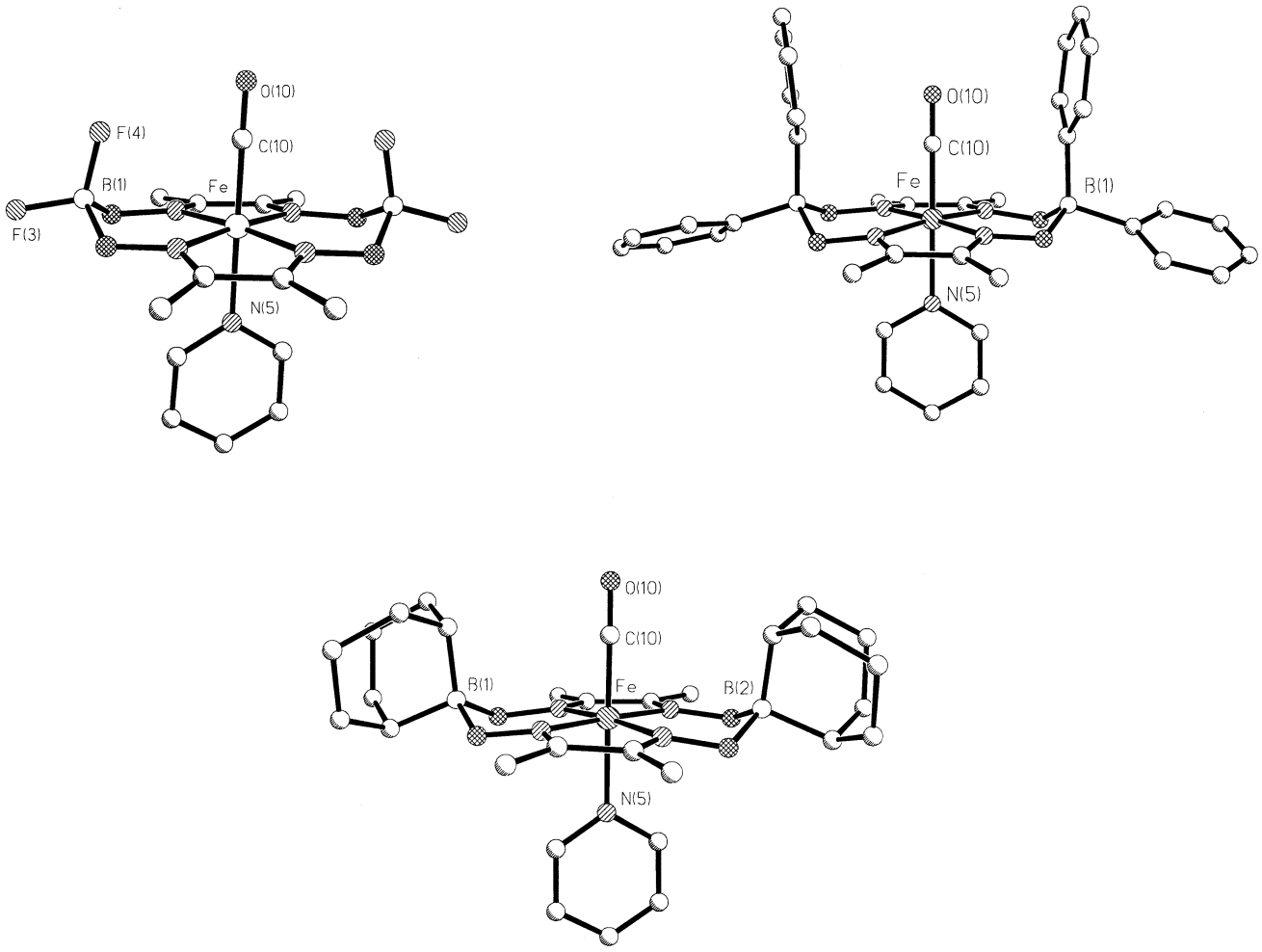

Fig. 2. X-ray structures of $Fe(DMGBR_2)_2(PY)(CO)$, $BR_2 = BF_2$, BPh_2, and BBN.

$Fe(DMGX)_2(PY)_2$	X = H 0.20 V, BBN 0.46 V, BH_2 0.61 V, BPh_2 0.62 V, BF_2 0.88 V
$Fe(DMGBPh_2)L_2$	L = NH_3 0.36 V, PY 0.62 V, CH_3CN 0.80 V
$Fe(DMGBPh_2)_2(PY)L$	L = CH_3CN 0.73 V, NPT 0.84 V, DDQ 1.09 V, TCNE 1.17 V

While the borylated oxime ligands favor the lower oxidation state of iron, the parent glyoximes ligand (DMGH) is known to stabilize higher oxidation states of metals. This arises because of the loss of the oximate proton giving a dianionic ligand as in the Ni(IV) derivative, $Ni(DMG)_3)^{2-}$ [24]. The borylated $[DMGBR_2]^-$ ligand retains the same overall anionic charge as the $DMGH^-$. Stabilization of the lower oxidation state is a result of the electron withdrawing character of the BF_2 group which puts the formal negative charge of $DMGBF_2^-$ on the boron atom and away from the metal.

3.1. Conformational features of borylated dioxime complexes [20,21]

The $Fe(DMGBR_2)_2LL'$ complexes adopt either the centrosymmetric C_{2h} conformation or the C_{2v} conformation depending upon the steric demands of the axial ligands. The favored conformation in solution ($L \neq L'$) can be reliably deduced in the BPh_2 system on the basis of ring current shifts of the ligand resonances in the ^{1}H-NMR as shown in Fig. 3.

Facile flips of the boroximate chelate rings interconvert C_{2h} and C_{2v} conformations and also serve to interchange axial and equatorial environments in C_{2h} structures of bis amine complexes. A rotation of the axial ligand bound to iron normally must accompany chelate ring flips in order to avoid prohibitive axial contacts, thus the term rotflip. Dynamic NMR methods establish a rate for the rotflip in $Fe(DMGBPh_2)_2$(*sec*-$BuNH_2)_2$ of ca. 5000 s^{-1} at 298 K [25]. This rate is much faster than the rate of ligand exchange. A splitting of DMG methyl ^{1}H-NMR resonances is evidence of slow rotation of 'sandwiched' TCNE and NPT ligands ($k < 1$

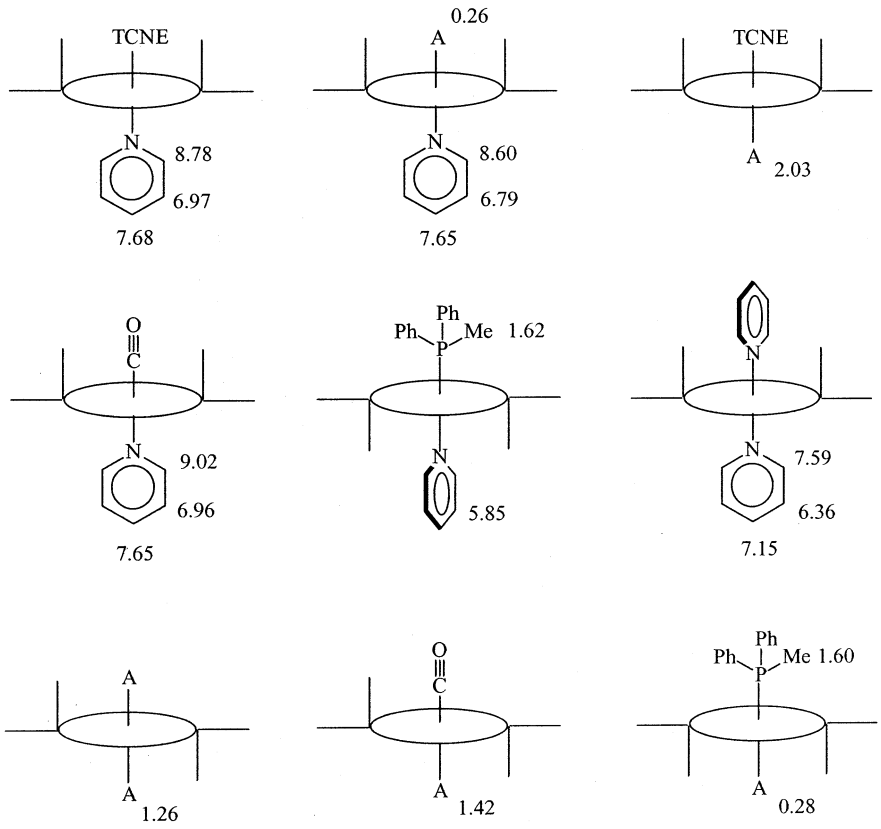

Fig. 3. Conformational preferences in $Fe(DMGBPh_2)_2$ complexes ($A = CH_3CN$). The ^{1}H-NMR shifts for for pyridine protons and methyl protons for CH_3CN and $PMePh_2$ ligands are given.

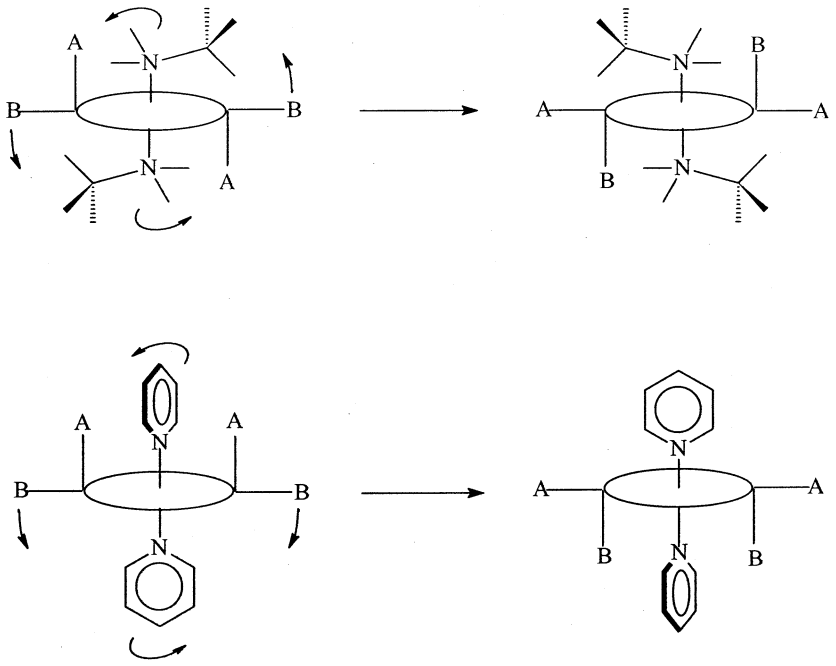

Fig. 4. Rotflips illustrated for the C_{2h} conformer of $Fe(DMGBPh_2)_2(i\text{-}PrNH_2)_2$ and C_{2v} conformer of $Fe(DMGBPh_2)_2(PY)_2$.

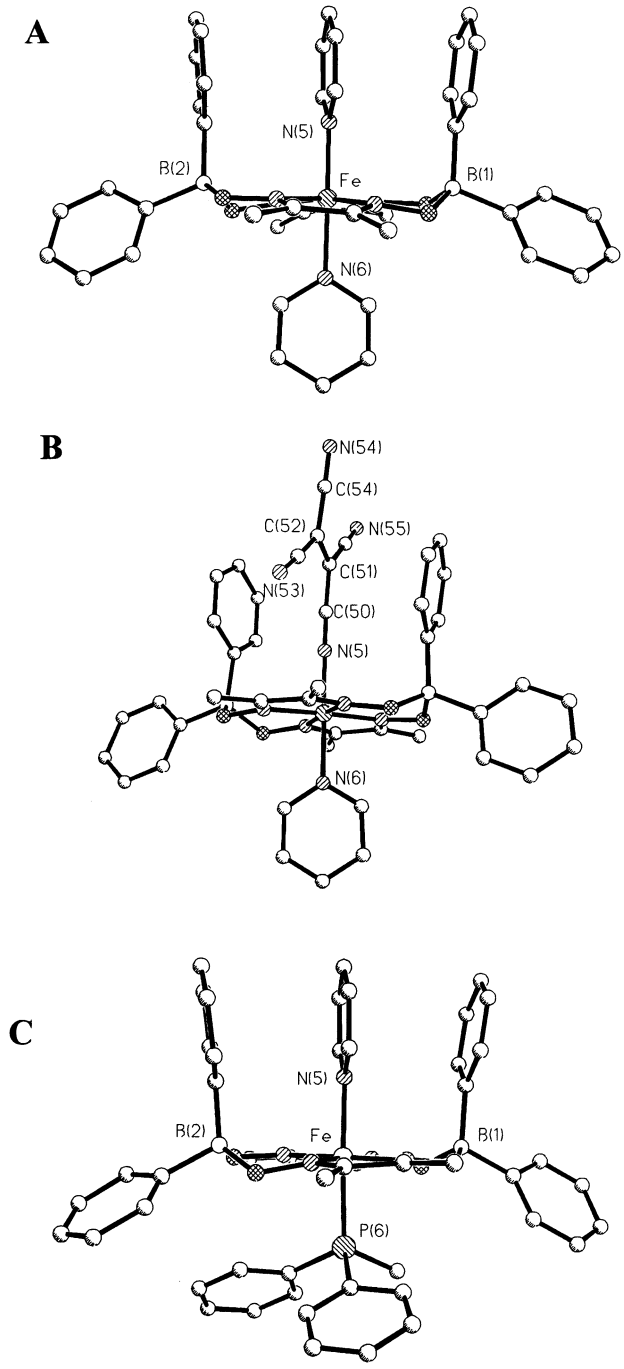

Fig. 5. Representative X-ray structures in C_{2v} conformations: (A) $Fe(DMGBPh_2)_2(PY)_2$; (B) $Fe(DMGBPh_2)_2(PY)(TCNE)$; (C) $Fe(DMGBPh_2)_2(PY)(PMePh_2)$.

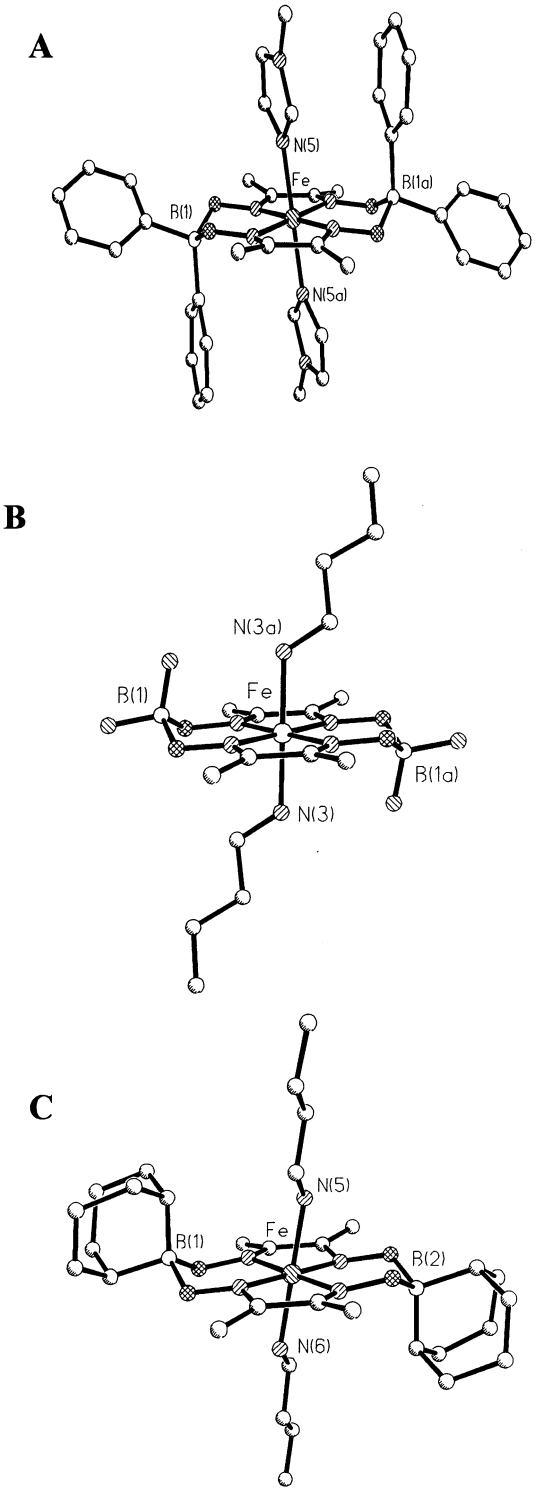

Fig. 6. Representative X-ray structures in C_{2h} conformations: (A) $Fe(DMGBPh_2)_2(MeIM)_2$; (B) $Fe(DMGBF_2)_2(BuNH_2)_2$; (C) $Fe(DMGBN)_2(BuNH_2)_2$.

s^{-1}) in the C_{2v} structures of $Fe(DMGBPh_2)_2(PY)(TCNE)$ $Fe(DMGBPh_2)_2(PY)(NPT)$.

The favored conformations for complexes where both axial ligands are the same ($L = L'$) cannot be reliably determined by NMR but are established on the basis of their crystal structures. Rapid rotflips produce a single set of average magnetic environments for axial and equatorial phenyl protons in C_{2h} structures. They also produce a single set of resonances for the distinctly different pyridine ligands in the C_{2v} structure. The rotflips are shown in Fig. 4.

The conformational dynamics and simplicity of the $Fe(DMGBPh_2)_2$ complexes are unique among systems which seek to mimic effects in heme proteins. In picket

Table 1
Structural comparison of C_{2h} $Fe(DMGBR_2)_2L_2$ structures [31]

R	BPh_2	BF_2	BBN	BPh_2	BPh_2	BPh_2	BF_2	BPh_2	BF_2	BPh_2	BF_2
L	$BuNH_2$	$BuNH_2$	$BuNH_2$	CH_3CN	PrCN	*i*-$PrNH_2$	*i*-$PrNH_2$	MeIm	Cl^-	PIP	PIP
FeN_4	1.884	1.877	1.895	1.898	1.886	1.89	1.885	2.89	1.898	1.89	1.883
Fe–L	2.053	2.047	2.036	1.941	1.926	2.046	2.063	2.02	2.233	2.16	2.132
δ Fe [a]	0.0	0.0	0.0	0.0	0.0	0.0	0.0	0.0	0.0	0.0	0.0
δ B[b]	0.36	0.48	0.27	0.45	0.37	0.46	0.44	0.30	0.30	0.31	0.40
ϕ [b]	56	13	75.5			11	76	67		83	67

Distances in Å (typically ±0.005 Å), angles in °.
[a] Displacement from mean N_4 plane.
[b] Average angle between a vertical plane through both boron atoms and the axial Fe–N–C_α plane.

fence porphyrins [26] and related heme models [27–29] a relatively rigid superstructure is created on one side of the heme plane in order protect the binding site or mimic effects of nonbonding interactions in heme proteins. These superstructures cannot be easily flipped to the opposite side and the conformational strain in them often complicates the interpretation of nonbonded effects on ligand binding. Among nonheme systems the lacunar tetraimine macrocycles developed by Busch must be noted. These incorporate conformationally complex superstructures in the vicinity of metal binding sites [30].

4. Crystal structures [31,32]

Representative X-ray structures are shown in the Figs. 2, 5 and 6. Structural data for complexes in the $Fe(DMGBF_2)_2$, $Fe(DMGBPh_2)_2$, and $Fe(DPGBF_2)_2$ systems are collected in Tables 1–3. All involve six-coordinate low spin Fe(II) except for $[Et_4N][Fe(DMGBF_2)_2Cl_2]$ which is a rare example of a low spin ferric chloro complex. The average Fe–N_4 bond lengths are consistently in the range 1.89 ± 0.01 Å. The 14-membered $[dioxBR_2]_2$ macrocycle has a smaller hole size than the porphyrins where Fe–N is typically 2.0 Å. Axial bond lengths are generally similar to those for heme analogues [33] even though as noted below their labilities are dramatically different.

The X-ray structures provide evidence of the two types of nonbonded interactions shown in Fig. 7. Axial effects refer to contacts between the axial ligands and axially directly B–R groups of the macrocycle. Face strain refers to contacts between the axial ligand and atoms within the plane of the N_4 macrocycle. The predominant facial contacts are with groups attached to the α-carbon of a bound amine ligand. The smaller hole size of the 14-membered dioxime macrocycles results in the facial effects being significantly greater than in the 16-membered porphyrins. Facial strain is greater over the five-membered diimine ring than over the six-membered boroximate rings.

The three carbonyl derivatives shown in Fig. 2 adopt the C_{2v} conformation. The CO ligand lies on the structured face in contact with the two axial boron substituents. The axial B–R substituents, which naturally pinch inward in six-membered rings, open with the increased size of R. The *trans* pyridine ligands adopt the same orientation in all three derivatives. The iron atom is displaced towards the CO ligand by 0.05–0.10 Å.

Table 2
Structural comparison of C_{2v} $Fe((DMG)BR_2)_2LT$ complexes [31]

	BPh_2	BF_2	BBN	BF_2	BPh_2	BPh_2	BPh_2	BPh_2	BF_2	BF_2
L	CO	CO	CO	CO	NH_3	TCNE	PY	PY	PY	4-*t*-BuPY
T	PY	PY	PY	*i*-$PrNH_2$	PY	PY	$PMePh_2$	PY	PY	4-*t*-BuPY
FeN_4 [a]	1.886	1.892	1.891	1.898	1.890	1.895	1.881	1.886	1.905	1.874
Fe–L [b]	1.789	1.772	1.771	1.793	2.03	1.850	2.055	1.999	2.055	2.027
Fe–T	2.067	2.055	2.068	2.100	2.04	2.018	2.298	2.051	2.048	2.030
δ Fe [c]	0.079	0.082	0.058	0.094	0.05	0.047	0.042	0.092	0.055	0.056
δ B [c]	0.45	0.59	0.37	0.57	0.45	0.50	0.33	0.43	0.49	0.47
ϕ T [d]	2.5	12.7	21.2	107.2	2.8	10.2		7.2	2.0	9.4
ϕ L[d]							78.8	79.8	81.5	83.3

[a] Average Fe–N_4 bond length
[b] Ligand bound inside cavity
[c] The maximum displacements of Fe and B atoms from mean N_4 plane are given.
[d] Angle between PY (or Fe–N–Cα) plane and vertical plane through boron atoms.

Table 3
Structural comparison of $Fe(DMGH)_2$, $Fe(DPGH)_2$, and $Fe(DPGBF_2)_2$ complexes

Complex	Conf.	FeN_4	Fe–L	δ Fe	δ B	ϕ [b]	Reference
$Fe(DMGH)_2(IM)_2$	Flat	1.905	1.985	0.0		6.9	[10]
$Fe(DPGH)_2(PY)_2$	Flat	1.910	2.030	0.0		20.5	[32]
$Fe(DPGBF_2)_2(PY)_2$	C_{2v}	1.893	2.037 [a], 2.044	0.057 [a]	0.58	77.9, 12.1	[32]
$Fe(DPGBF_2)_2(4\text{-}NH_2\ PY)_2$	C_{2v}	1.866	1.979 [a], 1.991	0.064	0.65	82.9, 2.0	[32]
$Fe(DPGBF_2)_2(BuNH_2)_2$	C_{2h}	1.872	2.036	0.0	0.53	67	[32]

[a] Ligand bound inside cavity.
[b] See footnote d in Table 2.

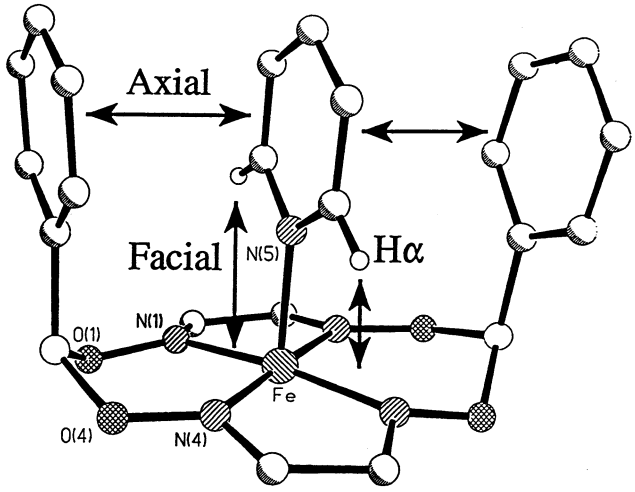

Fig. 7. Axial and facial strains in $Fe(DMGBPh_2)_2(PY)_2$.

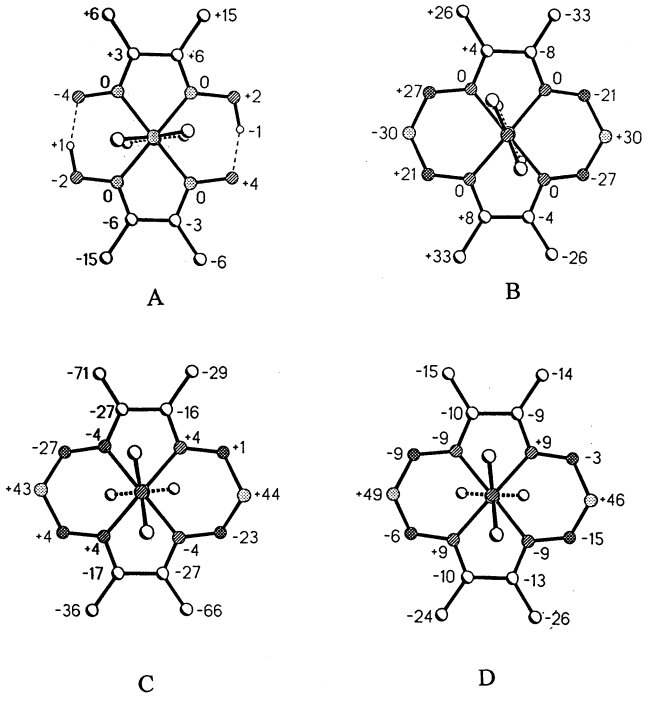

Fig. 8. Axial ligand orientation and macrocycle distortions in selected complexes. Perpendicular displacement of ring atoms, in units of 0.01 Å, from the mean N_4 plane are given. (+) is toward the cavity in C_{2v} cases: (A) $Fe(DMGH)_2(IM)_2$; (B) $Fe(DMGBPh_2)_2(MeIm)_2$; (C) $Fe(DMGBPh_2)_2(PY)_2$; (D) $Fe(DMGBF_2)_2(PY)_2$.

Additional C_{2v} structures are shown in Fig. 5. Ligands bound inside the cyclophane-like cavity are in close contact with both axial phenyl groups and lie in a plane parallel to them. The width of the cavity, as measured at the para carbon atoms, is 6.6 Å in the TCNE complex and 7.2 Å in the $PMePh_2$ and bis-PY complexes. The TCNE ligand is bound through a single nitrile group with the lower half in intimate contact with the axial phenyls.

Representative C_{2h} structures are shown in Fig. 6. These complexes are centrosymmetric with the iron atom centered in the N_4 plane. One boroximate ring is flipped up and the other down putting the two axial ligands in identical environments with each in close contact with a single B–R group. Evidence of axial strain is found in a tilting of the Fe–L bond axis away from the BR group.

4.1. Axial ligand orientation

Axial ligand orientations for some imidazole and pyridine derivatives are shown in Fig. 8. A combination of axial and facial effects serve to determine the orientation of the axial ligands. In $Fe(DMGH)_2$ or on the open face of the C_{2v} structures of $Fe(DMGBF)_2(PY)_2$ and $Fe(DMGBPh)_2(PY)_2$ ligands lie over the dioximate rings in order to minimize face strain. When bound on a structured face of the complex the pyridine or imidazole ligand is constrained to lie over the diimine rings.

Face strain effects explain why $Fe(DMGBR_2)_2(PY)_2$ complexes adopt the C_{2v} conformation while the similar $Fe(DMGBPh_2)_2(MeIM)_2$ adopts the C_{2h} structure. The α-C–H groups in the six-membered heterocyclic ligand (PY) lie almost 0.3 Å nearer to the macrocycle plane than in a similarly bound five-membered heterocycle (MeIM) ligand. In the C_{2v} conformation the pyridines lie in mutually perpendicular planes, thus permitting face strain relief via the distortions shown. In the C_{2h} structure the coplanar pyridine ligands would exert opposing pressures on the diimine chelate rings requiring prohibitive Fe–N bond lengthening. Weakly attractive N–H–F and N–H-π forces are indicated in structures involving the primary amine ligands $BuNH_2$, i-$PrNH_2$, and pip. These produce the orienta-

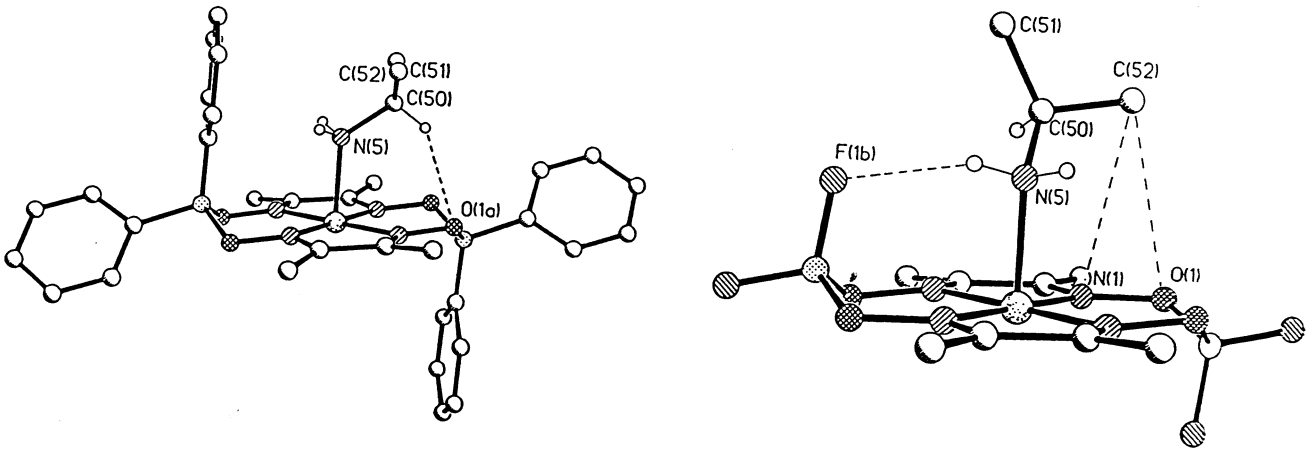

Fig. 9. Orientation of i-$PrNH_2$ ligand in $Fe(DMGBPh_2)_2(i\text{-}PrNH_2)_2$ and $Fe(DMGBPh_2)_2(i\text{-}PrNH_2)_2$. Some important nonbonded contacts are shown.

tions shown in Fig. 9 and result in an unusual eclipsed geometry of the i-$PrNH_2$ ligand in the BPh_2 derivative.

5. Kinetic and thermodynamic aspects of axial ligand binding to low spin Fe(II)

The FeN_4 systems bind virtually all common monodentate ligands giving low spin six-coordinate FeN_4L_2 and FeN_4LL' complexes. Ligand substitution reactions proceed via a classic dissociative (D) mechanism [11,12,19]. Reactions are accompanied by distinctive color changes and are easily monitored using spectrophotometric methods. A large body of rate and equilibria data for ligand binding has been accumulated in the $Fe(dioxH)_2$, $Fe(dioxBF_2)_2$, and $Fe(DMGBPh_2)_2$ systems (diox = dmg, bqd, and npq). The solubility in noncoordinating solvents such as dichloromethane or toluene avoids complications of solvent intervention and solvent effects are minimal.

The rate constants for ligand dissociation, k_{-L}, provide a direct measure of the relative binding strengths of ligands. Trends in k_{-L} as a function of the dioxime, BR_2 substitution, leaving group, L and *trans* ligand T have been elucidated. The dioxime systems are the most inert of the *trans*-FeN_4L_2 complexes studied to date (N_4 being any planar tetradentate macrocycle) while hemes are the most labile. Typically the DMG complex is 3–5 orders of magnitude more inert than the corresponding heme complex. Within the dioxime systems the relative lability order is DMG < NPQ ≪ BQD [19]. The boron substituents have a minimal electronic effect on ligation but lead to large nonbonded effects in the BPh_2 and BBN cases.

Table 4
Dissociation rate constants and bond lengths for FeN_4 complexes

Complex	$Fe(DMGBPh_2)_2$		$Fe(DMGBF_2)_2$		FeTPP	
	k_{-L} (s^{-1})	Fe–L_{ax} (Å)	k_{-L} (s^{-1})	Fe–L_{ax} (Å)	k_{-L} (s^{-1})	Fe–L_{ax} (Å)
$FeN_4(BuNH_2)_2$	0.013	2.053	0.013	2.047		2.039 [c]
$FeN_4(i\text{-}PrNH_2)_2$	1.0	2.046	1.0	2.063		
$FeN_4(PIP)_2$	76	2.16	16	2.132	$>10^4$ [b]	2.127 [d]
$FeN_4(MeIM)_2$	0.008	2.02	0.0013		1500 [b]	2.014 [d]
$FeN_4(PY)_2$	6.5	1.999 [a]	0.15	2.048 [a]		2.037 [e]
$FeN_4(PY)$	$<10^{-5}$	2.067	$<10^{-5}$	2.055		2.10 [d]
$FeN_4(CO)$	6×10^{-5}	1.789	2×10^{-5}	1.772	−0.02 [b]	1.77
$FeN_4(PY)$		2.018	–			
$FeN_4(TCNE)$	6×10^{-4}	1.850	4			
$FeN_4(CH_3CN)_2$	>1000	1.941	1000			

At 298 K, CH_2Cl_2 or toluene solution; Ref. [31].
[a] Ligand bound inside cavity.
[b] Estimates based on data for related hemes in Refs. [52,53].
[c] Ref. [54].
[d] Ref. [33]
[e] Ref. [55].

Table 5
$-\Delta G^{\circ}_{298}$ (kcal mol^{-1}) for Fe(DMGBR$_2$)$_2$ (PY)L complexes in CH_2Cl_2 [37]

L	BF_2	BPh_2	$\Delta\Delta G^{\circ}_{298}$
PY	9.07	6.38	2.7
PhCN	6.02	4.06	2
2-CNPY [a]	6.1	4.52	1.6
CH_3CN	5.8	5.56	0.2
CO	12.6	12.9	−0.3
PT	6.1	7	−0.9
2-CNPYMe$^+$	6.1	7.47	−1.4
MePZ$^+$	7.7	9.57	−1.9
NPT	6.1	8.2	−2.1
DDQ	7.1	10.9	−3.8
TCNE	7.9	12.5	−4.6

$-\Delta G^{\circ}_{298}$ is the free energy of formation relative to a value of 0.0 for the Fe(DMGBR$_2$)$_2$(CH_3CN)$_2$ complexes. A positive $\Delta\Delta G^{\circ}$ implies a repulsive phenyl-L interaction, a negative $\Delta\Delta G^{\circ}$ attractive.
[a] Binds via the nitrile nitrogen.

For Fe(DMGBF$_2$)$_2$ complexes the axial lability order is: THF > DMSO > CH_3CN > 2-MeIM > PY > 1-MeIM > P(OEt)$_3$ > RNC > CO [34–36]. Rate constants in the Fe(DMGBF$_2$)$_2$ TL complexes span over 10 orders of magnitude from ca. 10^{+6} s^{-1} for L = THF to ca. 10^{-5} s^{-1} for L = CO. Ligand lability also depends on a *trans* effect. The rate constant for CH_3CN loss from Fe(DMGBF$_2$)$_2$L(CH_3CN) spans a range from 10^{+5} s^{-1} *trans* to Br$^-$ to 10^{-3} s^{-1} trans to CO. The *trans* effect order for k_{-CH_3CN} is: Br$^-$ > Cl$^-$ > CH_3CN > PY > MeIM > PR_3 > P(OEt)$_3$ > RNC > CO [36].

The *trans* effect in these octahedral complexes is equal to or greater in magnitude to the classic *trans* effect in square planar Pt(II) complexes. π-Bonding is a predominant factor in both square planar and octahedral *trans* effects but it works in opposite directions. π-Acceptor ligands labilize the *trans* ligand in square planar systems by stabilizing the pentacoordinate intermediate in an associative (A) process. In FeN_4LT systems π-acceptors destabilize the dissociative pentacoordinate intermediate and therefore delabilize the trans ligand. In simple terms, π-acceptors facilitate additional bond making (A mechanism) but make bond breaking (D mechanism) more difficult. π-Donors such as halides or oxo groups have the opposite effect.

5.1. Structure reactivity relationships

In Table 4, some ligand dissociation rate constants are compared with the crystallographically determined metal ligand bond lengths for various FeN_4LL' complexes. Trends in ligand lability are not generally evident in the metal ligand bond lengths. Hemes are 10^3–10^5 times more labile than the Fe(DMGBR$_2$)$_2$ analogues but have similar or slightly shorter Fe-axial ligand bond lengths. Amine ligands bound *trans* to CO are more inert but have longer Fe–N bonds than when *trans* to another amine.

The lability order pip > *i*-PrNH$_2$ > BuNH$_2$ and PY > MeIm follows the order expected on the basis of steric effects but only in the case of piperidine is this clearly manifested in Fe–N bond lengthening. For other primary amine ligands steric strain is taken up by distortions of the macrocycle or axial ligand as described above. The bond lengths of the distinctly different pyridine ligands in the bis pyridine structures are a consequence of subtle differences in face and axial strain relief in the C_{2v} structures. Attractive nonbonded interactions such as the TCNE–phenyl interactions in Fe(DMGBPh$_2$)$_2$(PY)(TCNE) have a profound effect on lability quite independent of the metal ligand bond length.

5.2. Quantifying nonbonded effects on ligation [37]

The ligand binding differences between the BF_2 and BPh_2 systems are largely determined by the axial nonbonded interactions. Therefore, the difference in ligation free energy provides a measure of these interactions. Table 5 summarizes this approach. The binding constants for a variety of ligands, L, are determined for N_4 = (DMGBPh$_2$)$_2$ and (DMGBF$_2$)$_2$ in dichloromethane solution.

$$FeN_4(CH_3CN)_2 + L \rightleftarrows FeN_4(CH_3CN)(L) + CH_3CN \quad (5)$$
$$FeN_4(CH_3CN)L + L \rightleftarrows FeN_4(L)_2 + CH_3CN \quad (6)$$
$$FeN_4(PY)_2 + L \rightleftarrows FeN_4(PY)(L) + PY \quad (7)$$

Ligation free energies, ΔG°_{298}, are obtained via a thermodynamic cycle assigning $\Delta G^{\circ} = 0$ for the $FeN_4(CH_3CN)_2$ complexes. The differences in free energies of ligation between the BF_2 and BPh_2 systems, $\Delta\Delta G^{\circ}_{298}$, are then taken as a measure of the energy of interaction between the ligand in question and the π faces of the phenyl groups. Ligands with regions of + surface charge density, such as TCNE and MePZ$^+$, or 2-CNMePY$^+$, show attractive interactions with the negative surface charge of the π face of the phenyl groups while those with negative surface charge such as PY, PhCN, or 2-CNPY give a repulsive contribution. Ligands with minimal interaction with the phenyl, such as CO or CH_3CN, give negligible differences.

6. Spectroscopy and photochemistry

The Fe(II) glyoxime complexes are intensely colored as a result of MLCT transitions with extinction coefficients typically in the range of 5000–10 000 M^{-1} cm^{-1}. The position of the MLCT bands are very dependent on the axial ligands and correlate with the effects of L on the Fe$^{+3/2}$ reduction potential or Lever's E_L parameters

[39]. The MLCT bands move to higher energies with axial π-acceptor ligands. The MLCT bands occur at much lower energies in more delocalized dioximes such as benzoquinone ($Fe(BQDBF_2)_2L_2$) or napthoquinone ($Fe(NPQBF_2)_2L_2$) dioxime complexes but retain essentially the same dependence on the axial ligand L [19]. Axial ligands including TCNE, nitrophthalonitrile, methylpyrazinium, and pyridines, which possess low lying vacant π* orbitals, give rise to additional metal to axial ligand charge transfer transitions (MA × CT) in the visible or near IR region [20,38]. Some representative spectral trends are summarized below.

axial pyridines in mutual perpendicular planes [19,31]. A dramatic feature of the $Fe(DMGBPh_2)_2$ (PY)(TCNE) complex is the presence of a TCNE–phenyl charge transfer transition at 520 nm [38]. This demonstrates how groups may be positioned in a well-defined geometry so as to observe interactions between them.

Borylation results in a ca. 50 cm^{-1} increase in CO stretching frequencies but has only small effects on the CO lability. Increases in ν_{CO} with changes in the dioxime however parallel the large increase in lability of CO in the order DMG < NPQ ≪ BQD [19].

Quantum yields for MLCT photosubstitution in

MLCT vs. diox (λ_{max}, nm)	DMG	NPQ	BQD
$Fe(dioxH)_2(MeIM)_2$	531	702	755
$Fe(dioxBF_2)_2$ $(MeIm)_2$	533	683	716
$Fe(dioxBF_2)_2(CH_3CN)_2$	445	568	596
$Fe(dioxBF_2)_2(MeIm)(CO)$	404	494	501

MLCT vs. L (λ_{max}, nm)	MeIm	PBu_3	CH_3CN	$P(OBu)_3$	BuNC	CO
$Fe(DMGBF_2)_2(MeIm)L$	533	505	480	475	457	404
$Fe(NPQBF_2)_2(MeIm)L$	683	639	630	600	584	494

MA × CT vs. L (λ_{max}, nm)	PY	2-CNPY	PT	NPT	2-CNPYMe$^+$	MePZ$^+$	TCNE	DDQ
$Fe(DMGBPh_2)(PY)L$	406	423	470	625	667	770	1092	1552

ν_{CO} vs. N_4 (cm^{-1})	$(DMGH)_2$	$(NPQH)_2$	$(BQDH)_2$	$(DMGBF_2)_2$	$(NPQBF_2)_2$	$(BQDBF_2)_2$
$FeN_4(PY)(CO)$ [19]	1985	2010	2028	2049	2062	2063

Borylation usually has only a small effect on the visible spectroscopy. One noticeable feature is a splitting of the MpyCT band in $Fe(DMGBR_2)_2(PY)_2$ complexes as a consequence of the enforced orientation of the two

$Fe(DMGH)_2$ and $Fe(NPQH)_2$ complexes are reported by Irwin [40] and Chen [41]. The quantum yields for CO photodissociation are close to unity, as found in hemes [42] and other low spin d^6 carbonyls [43], even though quite different transitions are involved. Ligand dissociation from a common triplet ligand field state is proposed. Quantum yields for ligand photodissociation

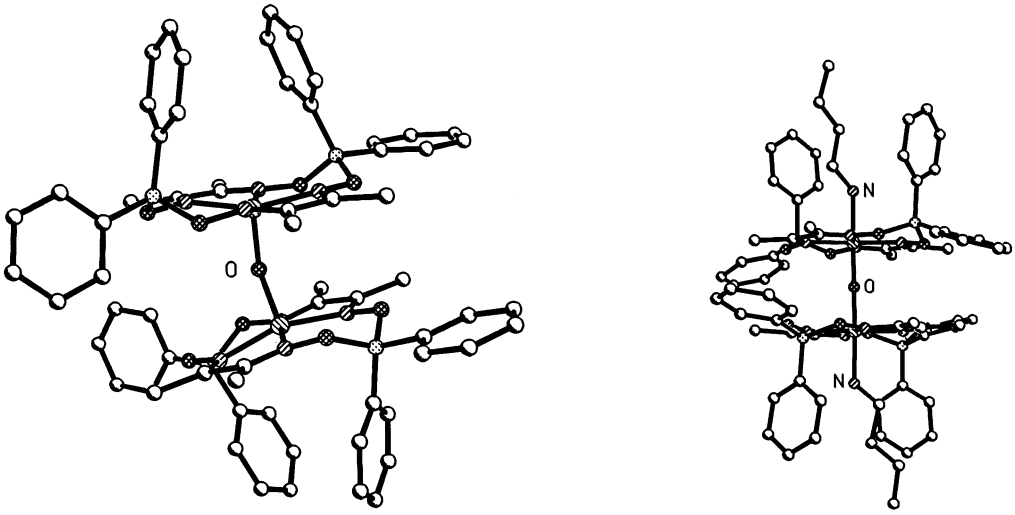

Fig. 10. X-ray Structures of $[Fe(DMGBPh_2)_2]_2O$ and $[(BuNH_2)Fe(DMGBPh_2)_2]_2O$.

correlate roughly with the π acceptor character of the ligands $CO > RNC > PR_3 > MeIM$. It was suggested that the order reflects the bond energy in the excited state. Population of the dz^2 orbital results in a severe lengthening of axial bonds (as found for example in Co(II) complexes). The π bonding is expected to be more sensitive to this elongation than the sigma bonding.

Flash photolysis of carbonyl derivatives has been used to measure the much more rapid reactions of weak ligand complexes involving CH_3CN, DMSO, THF, etc. [20,35]. All of the complexes containing photolabile ligands, X, show photochromism in solution based on the reversible shift of the equilibrium [41].

$$FeN_4LX + L \rightleftarrows FeN_4L_2 + X \quad (8)$$

The Fe(III) complexes are colored as a result of LMCT transitions but the known Fe(III) bis-dioxime complexes are limited to halides, pseudohalides, and μ-oxo complexes. In the μ-oxo species, $[LFeN_4]_2O$, transitions assigned to oxo to iron are found in the region (650–850 nm) depending upon the trans ligand L [44]. These transitions extend even farther into the near IR region in the trinuclear μ-oxo species $[LFeN_4O]_2RuTPP'$ [45,46].

7. Oxo bridged complexes

The μ-oxo diiron $[Fe_2O]$ unit is an important feature of the chemistry of iron [47] but has only recently been found for iron dioximes [44,48–50]. The μ-oxo dioxime systems are obtained by aerobic oxidation of the labile $Fe(DMGBR_2)_2(CH_3CN)_2$ complexes in dilute noncoordinating solvents such as dichloromethane. The oxidation is completely suppressed at $[CH_3CN] > 0.01$ M. The resulting diamagnetic yellow–brown solutions immediately become green and paramagnetic on subsequent addition of CH_3CN or other ligands. The changes in color and magnetism are a result of ligation *trans* to the oxo bridge.

Three different forms (unligated, mono and diligated) are characterized in the BPh_2 system and equilibrium constants for a variety of nitrile and amine ligands are reported [48].

$$FeN_4–O–FeN_4 + L \rightleftarrows LFeN_4–O–FeN_4 \quad (9)$$

$$LFeN_4–O–FeN_4 + L \rightleftarrows LFeN_4–O–FeN_4L \quad (10)$$

The structures of the fully ligated and unligated forms of $Fe(DMGBPh_2)_2$ (Fig. 10) reveal dramatic changes both in the primary coordination sphere and in the

Table 6
Structural data (Å, °) for μ-oxo diiron $[Fe_2O]$ complexes [49]

Complex	Fe–N_4	Fe–O	FeOFe	δ Fe [a]	Reference
$[Fe(DMGBPh_2)_2]_2O$	1.91	1.709	166	0.3	[49]
$[(BuNH_2)Fe(DMGBPh_2)_2]_2$ O	1.89	1.766	178.6	0.03	[49]
$[(MeIM)Fe(PC)]_2O$	1.92	1.749	175.1	0.02	[56]
$[Fe(t\text{-}Bu–PC)]_2O$	2.06	1.748	178.5	0.61	[57]
$[(H_2O)Fe(Me_2BBZ)]_2O$		1.759	175		[58]
$[Fe(TPP)]_2O$	2.09	1.763	174.5	0.54	[59]
$[Fe(OEP)]_2O$	2.08	1.756	172.2	0.5	[60]
$[Fe(salen)]_2O$		1.78	144.6	0.58	[61]

[a] Displacement of Fe toward oxo ligand is measured from mean N_4 plane for DMG BR_2 cases and mean macrocyclic core in other cases.

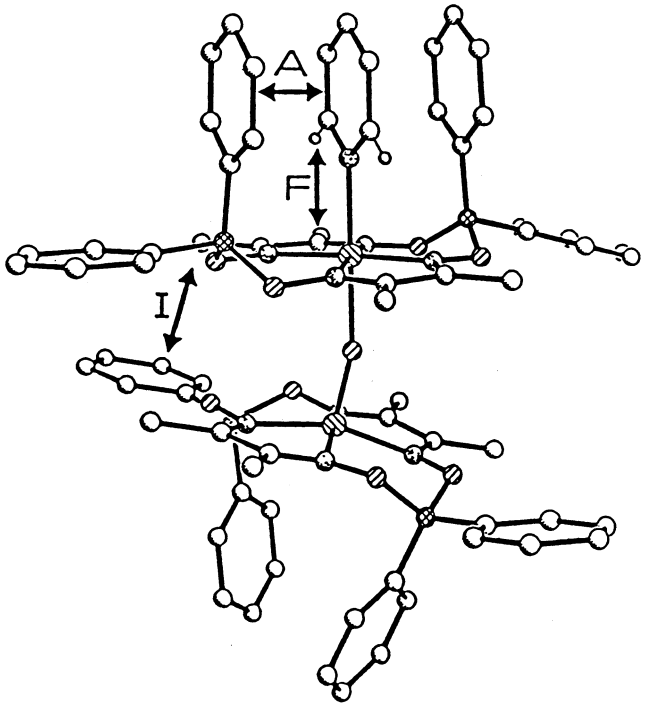

Fig. 11. Proposed structure of $[Fe(DMGBPh_2)_2]_2O$ monopyridine complex. Axial, facial and interfacial strains combine to reduce the affinity for a second pyridine ligand.

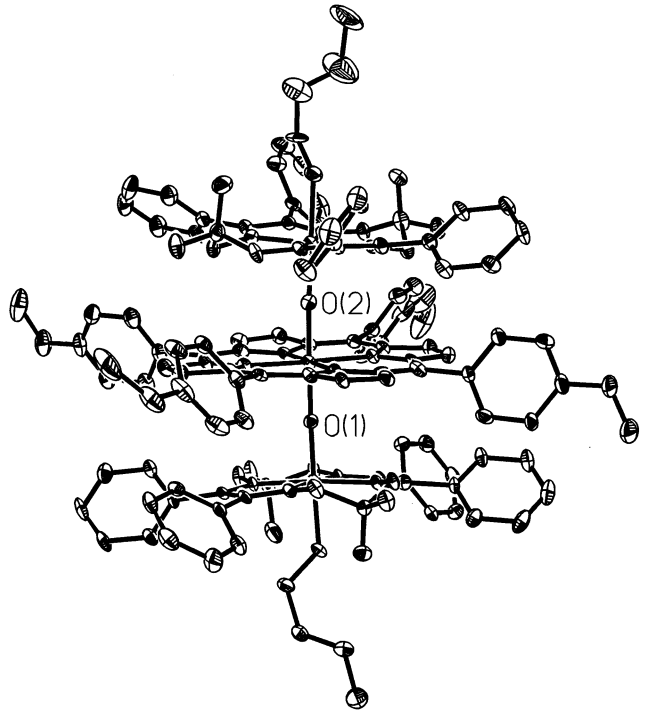

Fig. 12. X-ray structure of the heterotrinuclear complex $[(BuNH_2)Fe(DPGBF_2)_2O]_2RuTPP'$.

peripheral structure of the N_4 macrocycle [49]. Upon ligation the iron moves into the N_4 plane and the axial phenyl groups which are collapsed over the vacant coordination sites open to accommodate the amine ligand. Structural data are compared with some related μ-oxo diiron complexes in Table 6.

Paramagnetic ^{1}H-NMR is a powerful tool for investigating the mono and di-ligated μ-oxo forms [48]. The DMG methyl resonances appear upfield of TMS. Axial ligand resonances experience contact and dipolar shifts. For amine ligands, distinct resonances for mono and diligated forms of $[Fe(DMGBPh_2)_2]_2O$ and for mixed ligated species $LFeN_4–O–FeN_4L'$ are observed. Axial ligand proton resonances lie in the slow exchange limit in the 400 MHz NMR spectra but ligation is complete on mixing ($10^4 > k > 0.1$ s^{-1}). For weaker ligands including nitriles, H_2O, and 2,6-dimethylpyrazine the ^{1}H-NMR spectra versus [L] are consistent with a dynamic average of the various ligated forms ($k > 10^4$ s^{-1}).

Stepwise ligation to $[Fe(DMGBPh_2)_2]_2O$ has been followed by both ^{1}H-NMR and spectrophotometric titration. Steric effects of the BPh_2 groups produce dramatic reductions in the second binding constant, K_2, for PY, *i*-$PrNH_2$, and piperidine. These are ligands which experience the greatest facial strain. The proposed steric factors are illustrated in Fig. 11. Binding at the second iron site is reduced owing to the effects of peripheral changes in structure which accompany ligation in the other subunit. Reductions in binding free energy at the second site are 6.1 kcal mol^{-1} for PY and 3.5 kcal mol^{-1} for *i*-$PrNH_2$. The changes have been compared to those responsible for the cooperative effects in hemoglobin. More importantly, they demonstrate how complex nonbonded effects can be achieved and understood in very simple systems.

7.1. Reactions of the μ-oxo complexes

The $[LFe(DMGBR_2)_2]_2O$ complexes are much stronger oxidants than μ-oxo hemes and will oxidize a variety of substrates including phosphines, sulfoxides, hydroquinones, catechols etc. [50,51]. The detailed kinetics of 4-*t*-butylcatechol (H_2Q) oxidation has been studied in dichloromethane solution.

$$LFeN_4–O–FeN_4L + H_2Q + 2L \Rightarrow 2FeN_4L_2 + H_2O + Q \quad (11)$$

A 1/[L] dependence of the rate suggests that the mechanism involves H-atom abstractions from a bent monoligated species (see Fig. 10) in the rate determining step. An interesting observation is that the rate of the redox step correlates with the ability of the trans ligand L, to stabilize the higher oxidation state. An asymmetric LFe(IV)–O–Fe(II) resonance form is suggested to explain the kinetics. The relative rates in reaction 11 are $DPGBF_2 > DMGBF_2 \gg DMGBPh_2$. It appears that the reactivity of the μ-oxo group is dependent upon the

ability of the N_4 macrocycle to fold back and thus permit bending of the Fe–O–Fe moiety [51].

The oxo bridge in $[Fe(DMGBF_2)_2]_2O$ is cleaved by acids in acetonitrile solution producing strongly oxidizing solutions believed to contain the ferric species $[Fe(DMGBF_2)_2(CH_3CN)_2]^+$. Reaction with anions gives stable ferric complexes displaying EPR spectra characteristic of low spin Fe(III) [19].

7.2. Trinuclear μ-oxo complexes

Reaction of $FeN_4(CH_3CN)_2$ complexes with dioxoruthenium(VI)porphyrins, $RuTPP'(O)_2$, tpp′ = tetrakis(4-methoxyphenylporphyrinate), affords novel diamagnetic heterotrinuclear complexes where FeN_4 may be $Fe(DMGBF_2)_2$, $Fe(DMGBPh_2)_2$, $Fe(DPGBF_2)_2$, or FePc [45,46].

$$2FeN_4(CH_3CN)_2 + RuTPP'(O)_2 \rightarrow [(CH_3CN)FeN_4O]_2RuTPP' + 2CH_3CN \quad (12)$$

A variety of ligated derivatives, $[LFeN_4{-}O]_2RuTPP'$ have been characterized in dichloromethane solution on the basis of distinctive near-IR spectra and ring current shifted ^{1}H-NMR spectra. In the crystal structure of the $[(BuNH_2)Fe(DPGBF_2)_2O]_2RuTPP'$ (Fig. 12) the iron is displaced 0.06 Å from the N_4 plane towards the oxo ligand with a nearly linear Fe–O–Ru–O geometry (FeORu 175°, Fe–O = 1.788 Å Ru–O = 1.80 Å [45]. The diamagnetism is consistent with a linear delocalized $d\pi^8$ system, formally Fe(III)–O–Ru(IV)–O–Fe(III).

The reaction of the trinuclear complexes with 4-*t*-butylcatechol (H_2Q) proceeds according to reaction (13) with relative rates $DPGBF_2 > DMGBF_2 \gg DMGBPh_2 \gg Pc$. This order parallels the reactivity of the binuclear $[FeN_4]_2O$ analogues.

$$RuTPP'[OFeN_4L]_2 + 2H_2Q + 2L \Rightarrow 2FeN_4L_2 + RuTPP'L_2 + H_2O + Q \quad (13)$$

8. Other metals

While dioxime complexes of numerous transition metals are known, only a few borylated systems are reported. Dreos et al. [62] have studied various diphenylborylated organocobaloximes and organorhodoximes. These display conformational features similar to those found in the iron systems. Novel dimeric organocobaloximes derived from 4-pyridylboronic acid have also been described [63].

9. Summary

The FeN_4 systems provide an extremely versatile set of inorganic complexes. Their chemistry bridges the gap between classical inert low spin d^6 systems such as cobalt(III) amines studied in aqueous solution and inert organometallic compounds which typically contain metals in low oxidation states and involving π-acceptor ligands. The complexes span an enormous range in redox potential, color, and lability. The large body of spectroscopic, kinetic, thermodynamic, and conformational data amassed over the past two decades forms a sound basis for applications which require the precise control of ligation, redox potential, absorption spectra, or the controlled mutual orientation of moieties.

Acknowledgements

The work described here could not have been done without the continued financial support of the Natural Sciences and Engineering Research Council of Canada and the dedicated efforts of numerous undergraduate scholars, graduate students, and postdoctoral associates whose names appear as coauthors in the references.

References

[1] A. Chakravorty, Coord. Chem. Rev. 13 (1974) 1.
[2] L.A. Tschugaev, Z. Anorg. Chem. 46 (1905) 144.
[3] J.H. Pratt, Inorganic Chemistry of Vitamin B-12, Academic Press, New York, 1972.
[4] (a) G.N. Schrauzer, Accs. Chem. Res. 1 (1968) 97; (b) G.N. Schrauzer, Angew. Chem. Int. Ed. Engl. 15 (1976) 417.
[5] B.A. Jilliot, R.J.P. Williams, J. Chem. Soc. (1958) 462.
[6] L. Vaska, T. Yamaji, Inorg. Chem. 93 (1971) 6673.
[7] K. Bowman, A.P. Gaughan, Z. Dori, J. Am. Chem. Soc. 94 (1972) 727.
[8] N. Sanders, P. Day, J. Chem. Soc. Sect. A (1969) 2303.
[9] Y. Yamano, I. Masudo, K. Shinra, Bull. Chem. Soc. Jpn. 4 (1971) 1581.
[10] B.W. Dale, R.J.P. Williams, P.R. Edwards, C.E. Johnson, Trans. Faraday Soc. 64 (1968) 620.
[11] I.W. Pang, D.V. Stynes, Inorg. Chem. 16 (1977) 590.
[12] X. Chen, D.V. Stynes, Inorg. Chem. 25 (1986) 1173.
[13] F. Pomposo, D.V. Stynes, Inorg. Chem. 22 (1983) 569.
[14] N. Siddiqui, D.V. Stynes, Inorg. Chem. 25 (1986) 1982.
[15] P. Lefko, D.V. Stynes, J. Coord. Chem. 16 (1988) 383.
[16] G.N. Schrauzer, Chem. Ber. 95 (1962) 1438.
[17] S.C. Jackels, N.J. Rose, Inorg. Chem. 12 (1973) 1232.
[18] Y.Z. Voloshin, O.A. Varzatskii, T.E. Kron, V.K. Belsky, V.E. Zavodnik, N.G. Strizhakova, A.V. Palchik, Inorg. Chem. 39 (2000) 1907 (and references cited therein).
[19] D.W. Thompson, D.V. Stynes, Inorg. Chem. 29 (1990) 3815.
[20] D.V. Stynes, D. Leznoff, D.G.A.H. de Silva, Inorg. Chem. 32 (1993) 3989.
[21] D.G.A.H. de Silva, D.B. Leznoff, G. Impey, I. Vernik, J. Zin, D.V. Stynes, Inorg. Chem. 34 (1995) 4015.
[22] M. Verhage, D.A. Hoogwater, H. van Beckum, J. Reedijk, Rec. Trav. Chim. 101 (1982) 351.

[23] J.C. Jansen, M. Verhage, Cryst. Struct. Commun. 11 (1982) 305.
[24] S. Acharya, G. Neogi, R.K. Panda, Inorg. Chem. 23 (1984) 4393.
[25] D.V. Stynes, N. Somers, I. Vernik, to be submitted.
[26] J.P. Collman, Accs. Chem. Res. 10 (1977) 265.
[27] C. Slebodnick, J.C. Fettinger, H.B. Peterson, J.A. Ibers, J. Am. Chem. Soc. 118 (1996) 3216 (and references therein).
[28] C. Portela, D. Magde, T.G. Traylor, Inorg. Chem. 32 (1993) 1313.
[29] T.G. Traylor, S. Tsuchiya, D. Campbell, M. Mitchell, D.V. Stynes, N. Koga, J. Am. Chem. Soc. 107 (1985) 604.
[30] W. Lin, N.W. Alcock, D.H. Busch, J. Am. Chem. Soc. 113 (1991) 7603.
[31] I. Vernik, D.V. Stynes, Inorg. Chem. 35 (1996) 6210.
[32] I. Vernik, MSc Thesis, York University, 1997.
[33] W.R. Scheidt, C.A. Reed, Chem. Rev. 81 (1981) 543.
[34] D.V. Stynes, D.G.A.H. deSilva, D.W. Thompson, Inorg. Chim. Acta 188 (1991) 139.
[35] D.W. Thompson, D.V. Stynes, Inorg. Chem. 30 (1991) 636.
[36] D.W. Thompson, D.G.A.H. de Silva, D.V. Stynes, Inorg. Chem. 30 (1991) 4586.
[37] D.V. Stynes, Inorg. Chem. 33 (1994) 5022.
[38] G. Impey, D.V. Stynes, J. Am. Chem. Soc. 115 (1993) 7868.
[39] A.B.P. Lever, Inorg. Chem. 29 (1990) 1271.
[40] C. Irwin, D.V. Stynes, Inorg. Chem. 17 (1978) 2682.
[41] D.V. Stynes, X. Chen, Inorg. Chem. 26 (1987) 3145.
[42] B.M. Hoffman, Q.H. Gibson, Proc. Natl. Acad. Sci. USA 78 (1981) 21.
[43] A. Butler, R.G. Linck, Inorg. Chem. 23 (1984) 4545.
[44] D.W. Thompson, H. Noglik, D.V. Stynes, Inorg. Chem. 30 (1991) 4567.
[45] I. Vernik, D.V. Stynes, Inorg. Chem. 37 (1998) 10.
[46] F. Zobi, D.V. Stynes, Can. J. Chem. 79 (2001) 795.
[47] D.M. Kurtz, Chem. Rev. 90 (1990) 585.
[48] I. Vernik, D.V. Stynes, Inorg. Chem. 35 (1996) 2011.
[49] I. Vernik, D.V. Stynes, Inorg. Chem. 35 (1996) 2006.
[50] H. Noglik, D.W. Thompson, D.V. Stynes, Inorg. Chem. 30 (1991) 4571.
[51] I. Vernik, D.V. Stynes, Inorg. Chem. 35 (1996) 1093.
[52] D.K. White, J.B. Cannon, T.G. Traylor, J. Am. Chem. Soc. 101 (1979) 2443.
[53] C. Tetreau, D. Lavelette, M. Momenteau, J. Am. Chem. Soc. 105 (1983) 1506.
[54] O. Monro, P. Sizwe Madlala, R.A.F. Warby, T. Seda, G. Hearne, Inorg. Chem. 39 (1999) 4724.
[55] N. Li, P. Coppens, J. Landman, Inorg. Chem. 27 (1988) 482.
[56] C. Ercolani, M. Gardini, K.S. Murray, S. Dzunga, V.L. Goedken, G. Pennesi, G. Rossi, J. Chem. Soc. Dalton Trans. (1991) 1309.
[57] M. Lausmann, I. Zimmer, J. Lex, H. Lueken, K. Wieghardt, E. Vogel, Angew. Chem. Int. Ed. Engl. 33 (1994) 736.
[58] P. Payra, S. Hung, W. Kwok, D. Johnston, J. Gallucci, M.L. Chan, Inorg. Chem. 40 (2001) 4036.
[59] P.N. Swepson, J.A. Ibers, Acta Crystallogr. Sect. C C41 (1985) 671.
[60] B. Cheng, J.D. Hobbs, G. Debrunner, J. Erlebacher, J. Shelnutt, W.R. Scheidt, Inorg. Chem. 34 (1995) 102.
[61] F. Corazza, C. Floriani, M. Zehnder, J. Chem. Soc. Dalton Trans. (1987) 709.
[62] (a) F. Asaro, R. Dreos, S. Geremia, G. Nardin, G. Pellizer, L. Randaccio, G. Tauzher, V. Sara, J. Organomet. Chem. 548 (1997) 211;
(b) R. Dreos, S. Geremia, G. Nardin, L. Randaccio, G. Tauzher, V. Sera, Inorg. Chim. Acta 272 (1998) 74;
(c) F. Asaro, R. Dreos, G. Nardin, G. Pellizer, S. Peressini, L. Randaccio, P. Siega, G. Tauzher, C. Tavagnacco, J. Organomet. Chem. 601 (2000) 114.
[63] (a) R. Dreos, G. Nardin, L. Randaccio, G. Tauzher, S. Vuano, Inorg. Chem. 36 (1997) 2463;
(b) R. Dreos, G. Nardin, L. Randaccio, P. Siega, G. Tauzher, V. Vrdoljak, Inorg. Chem. 40 (2001) 5536.